14th World Congress on Computational Mechanics (WCCM)
ECCOMAS Congress 2020)
Virtual Congress: 11-–15 January 2021
F. Chinesta, R. Abgrall, O. Allix and M. Kaliske (Eds)

MODEL ORDER REDUCED TRANSIENT ACOUSTIC FINITE ELEMENT SIMULATIONS WITH IMPEDANCE BOUNDARY CONDITIONS

MAX MILLER III[1,3], SJOERD VAN OPHEM[1,3], ELKE DECKERS[2,3] AND WIM DESMET[1,3]

[1] KU Leuven, Department of Mechanical Engineering
Celestijnenlaan 300 B, B-3001 Heverlee, Belgium
{max.milleriii, sjoerd.vanophem, wim.desmet}@kuleuven.be

[2]KU Leuven, Diepenbeek Campus, Department of Mechanical Engineering
Wetenschapspark 27, 3590 Diepenbeek, Belgium
elke.deckers@kuleuven.be

[3] DMMS Lab, Flanders Make, Belgium

Key words: MOR, TDIBC, FEM, transient, acoustic, reduced

Abstract. The efficiency of time-domain acoustic simulations is improved immensely if the degrees of freedom imparted by the spatial discretization are reduced. Time-stable model order reduction strategies achieve this by ensuring that frequency-domain system realizations transform in a physical manner after reduction. Frequency dependent damping matrices add to the challenge and require additional consideration. Handling the associated boundary condition imposition in the time domain is one way to approach the problem. Convolution complicates this strategy but the obstacle can be surmounted using a recursive formulation. This work proposes such a method, combining Krylov subspace projection based model order reduction with an efficient time domain-impedance boundary condition implementation. The mass and stiffness matrices are frequency independent and reduced using a second-order Arnoldi algorithm. As Arnoldi iterations implicitly match the moments of the system transfer function, the complex damping matrix must still be contended with. Discussion is included on when reduced order, time-domain, simulations bear fruit. Comparison with full-order time and frequency-domain calculations demonstrate the effectiveness of the proposed algorithms with system degrees of freedom decreased from NDOF= 13125 to RDOF= 63, and simulation time reductions of 91–97%.

1 INTRODUCTION

Modeling the intricate microstructure of a porous/fibrous material is cost prohibitive in acoustic simulations. Impedance boundary conditions instead allow a surface to reflect and absorb sound energy, often to a suitable degree of accuracy. These complicated materials respond to incident perturbations over a variety of time-scales. In the frequency domain this leads to impedance functions that vary with frequency. Further shaping the frequency response is the thickness of the boundary layer which can be accounted for using a transfer matrix and an appropriate complex propagation coefficient [1]. In the frequency

domain this is all well and good, in the time domain calculating numerous convolutions proves costly. Time-domain impedance boundary conditions (TDIBC), defined by recursively calculated convolutions, provide an economical way to proceed [2, 3, 4, 5, 6, 7].

In combination with a TDIBC formulation, a method to reduce the problem degrees of freedom (DOF) is sought. While projection based model order reduction (MOR), guided by the system transfer function, is effective for transient problems, special care is required for construction of the reduction basis. This work builds on MOR techniques that require time-domain stability from the outset [8, 9], and a strategy to accommodate frequency dependent damping while allowing iterative, numerically sound, construction of the reduction basis [10, 11].

A MOR strategy and TDIBC enables transient acoustic simulations where both efficiency and accuracy are required. Of particular interest is the ability to directly output binaural audio from the simulations whereby a dry input signal (recorded under anechoic conditions) is effectively filtered by the linear time invariant (LTI) system under consideration.

In Sect. 2 the problem is described and a time-domain impedance boundary condition is developed for acoustic finite element methods. Section 3 discusses how to iteratively construct a reduction basis which spans a Krylov subspace using a modified second-order Arnoldi algorithm (SOAR) [12, 10]. Section 4 handles the numerical verification strategy while Sect. 5 presents the associated results.

2 PROBLEM DESCRIPTION

This work makes use of the surface normal acoustic impedance, $\boldsymbol{Z}_s(s)$, and the reciprocal specific normal acoustic admittance, $\boldsymbol{Y}_s(s)$, with

$$\boldsymbol{Z}_s(s)^{-1} = \boldsymbol{Y}_s(s) = \frac{\boldsymbol{V}(s)}{\boldsymbol{P}(s)} = \frac{\boldsymbol{A}(s)}{\dot{\boldsymbol{P}}(s)} = \mathcal{L}\left\{y_s(t)\right\}. \tag{1}$$

The symbol $\mathcal{L}\{\cdot\}$ represents the Laplace transform operator, $\boldsymbol{V}(s)$ is the surface normal particle velocity, $\boldsymbol{A}(s)$ is the surface normal particle acceleration, $\boldsymbol{P}(s)$ is pressure, and $\dot{\boldsymbol{P}}(s)$ is the time derivative of pressure. The time-domain counterparts will be written as lowercase functions of time, $\boldsymbol{v}(t)$, $\boldsymbol{a}(t)$, $\boldsymbol{p}(t)$, and $\dot{\boldsymbol{p}}(s)$, respectively. Working with $\boldsymbol{Z}_s(s)$ at the impedance boundary, Γ_z in Fig. 1, requires a locally reacting assumption whereby incident sound waves refract in the direction of the surface normal vector, $\boldsymbol{n}$. The degree to which this is a good approximation depends on the material, see [13] for a discussion and experimental results. The material under consideration for this work, high flow resistivity mineral wool, is suitable for use with this assumption. The three-dimensional, interior acoustic, problem under consideration is additionally defined by the fluid volume, Ω, Neumann boundary, Γ_N, and Dirichlet boundary, Γ_D.

The acoustic wave equation which dictates the finite element formulation is

$$\nabla^2 \boldsymbol{p}(\boldsymbol{x},t) - \frac{1}{{c_0}^2}\ddot{\boldsymbol{p}}(\boldsymbol{x},t) = -\boldsymbol{Q}(\boldsymbol{x},t), \tag{2}$$

here c_0 is the speed of sound in air, ∇^2 is the Laplacian, and $\boldsymbol{Q}(\boldsymbol{x},t)$ is a source term, a function of both space and time. The finite element formulation in the time domain is written as [14]

$$\mathbf{M}\ddot{\boldsymbol{p}}(t) + \mathbf{C}\dot{\boldsymbol{p}}(t) + \mathbf{K}\boldsymbol{p}(t) = \boldsymbol{f}^{ext}(t). \tag{3}$$

where $\mathbf{K}, \mathbf{C}, \mathbf{M} \in \mathbb{R}^{\mathrm{NDOF} \times \mathrm{NDOF}}$ are the stiffness, damping and mass matrices, respectively, and $\boldsymbol{f}^{ext} \in \mathbb{R}^{\mathrm{NDOF} \times 1}$ is the input load vector.

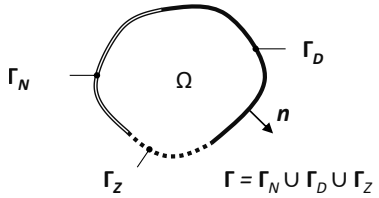

Figure 1: The interior acoustic problem. The fluid domain Ω with impedance, Neumann, and Dirichlet boundaries $\Gamma_Z, \Gamma_N, \Gamma_D$, respectively.

When the damping matrix is a function of frequency, the term $\mathbf{C}\dot{\boldsymbol{p}}(t)$ becomes a damping force vector, $\boldsymbol{f}^d$, where convolutions are required for the DOFs on Γ_Z,

$$\boldsymbol{f}_i^d = \rho_0 S_i y_s(t)_i * \dot{p}_i(t) = \rho_0 S_i a_i(t). \tag{4}$$

here the area associated with i'th boundary node is S_i, the normal particle acceleration is a_i, and the operator for convolution is $*$. As pointed out in the introduction, the convolutions can prove costly in terms of memory and computational burden.

A minimal memory, recursively calculated treatment of the convolutions is desired. First, a rational function is used to fit the Laplace domain admittance

$$\boldsymbol{Y}_s(s) \approx \sum_{k=1}^{N_\xi} \frac{\mu_k}{s - \xi_k}, \tag{5}$$

where ξ_k are the poles of the approximations, and μ_k are the gains. To insure time-domain stability, the algorithm *vectfit3* is used in the present work [15, 16, 17, 18]. The inverse Laplace transform of Eq. (5) is

$$\boldsymbol{y}_s(t) \approx \sum_{k=1}^{N_\xi} \mu_k e^{\xi_k t} \boldsymbol{H}(t), \tag{6}$$

where $\boldsymbol{H}(t)$ is the Heaviside or unit step function. Note that the time dependence of the admittance kernel is now determined no matter the problem of interest. The pressure derivative convolves with the admittance kernel, as shown in Eq. (4),

$$\boldsymbol{a}(t) = \boldsymbol{y}_s(t) * \dot{\boldsymbol{p}}(t) \approx \sum_{k=1}^{N_\xi} \mu_k \boldsymbol{\phi_k}(t) \tag{7}$$

to arrive at an expression for the particle acceleration. The variables $\boldsymbol{\phi}_k$ are introduced and are defined by

$$\boldsymbol{\phi}_k(t) = e^{\xi_k t} * \dot{\boldsymbol{p}}(t) + \boldsymbol{\phi_k}(0) e^{\xi_k t}. \tag{8}$$

A discrete version of Eq. (8) is determined by taking the pressure derivative as constant during the time step to arrive at

$$\boldsymbol{\phi}_{n+1}^k = \phi_n^k e^{\xi_k \Delta t} - \frac{1}{\xi_k}\left(1 - e^{\xi_k \Delta t}\right) \dot{\boldsymbol{p}}_{n+1}, \tag{9}$$

see [4, 7, 19] for more details. The variables $\boldsymbol{\phi}_k$ are known by different names in the literature, all of which allude to a characteristic preservation of information property. In [2] the authors expound upon this in an illuminating way.

3 MODEL ORDER REDUCTION

To decrease the system size, a structure preserving second-order Arnoldi method (SOAR) is taken as the starting point [10, 12]. The principle idea is to expand the system transfer function around various expansion points, s_0, to an appropriate order. The desired basis vectors, termed moments, are the coefficients of the Taylor series expansion. A couple of challenges arise, the first being explicit calculation of the transfer function moments proves to be numerically unstable [20]. An implicit method of basis construction is then desired. Unique system transfer functions arise depending on the problem of interest. In the present case, frequency dependency in the damping matrix and the consideration of arbitrary expansion points dictate modifications to previously proposed iterative algorithms. This work proceeds in the manner of [10] and [11].

The goal is to determine constant (at a given expansion point) coefficient matrices $\mathbf{A_1}$ and $\mathbf{A_2}$, as well as a starting vector $\boldsymbol{b}$ to allow calculation of the reduction basis

$$\mathcal{K}_n(\mathbf{A_1}, \mathbf{A_2}, \boldsymbol{b}) = \text{span}\{\boldsymbol{q}_0, \boldsymbol{q}_1, ...\boldsymbol{q}_{n-1}\} = \text{span}\{\mathbf{V}\}, \tag{10}$$

using the recurrence relations [10]

$$\begin{aligned} &\boldsymbol{q}_0 = \boldsymbol{b},\ \boldsymbol{q}_1 = \mathbf{A_1}\boldsymbol{b}, \\ &\boldsymbol{q}_n = \mathbf{A_1}\boldsymbol{q}_{n-1} + \mathbf{A_2}\boldsymbol{q}_{n-2}. \end{aligned} \tag{11}$$

To prevent a singular reduction basis, each new vector, $\boldsymbol{q_i}$, is orthonormalized with respect to the previously calculated basis vectors, resulting in the vector $\boldsymbol{v}_i$. These vectors span a Krylov subspace and form the projection matrix $\mathbf{V} \in \mathbb{C}^{\text{NDOF}\times\text{RDOF}}$. To determine $\mathbf{A_1}$, $\mathbf{A_2}$ and the starting vector $\boldsymbol{b}$, a decision is required as to whether the input or output Krylov subspace is to be spanned. The input and output subspaces for a standard, zero-centered, transfer function based off the frequency-independent system in Eq. (3), are defined by $\mathcal{K}_n(-\mathbf{K}^{-1}\mathbf{C}, -\mathbf{K}^{-1}\mathbf{M}, -\mathbf{K}^{-1}\tilde{\boldsymbol{b}})$ and $\mathcal{K}_n(-\mathbf{K}^{-\text{T}}\mathbf{C}^{\text{T}}, -\mathbf{K}^{-\text{T}}\mathbf{M}^{\text{T}}, -\mathbf{K}^{-\text{T}}\tilde{\boldsymbol{c}})$, respectively. Replacement matrices $\tilde{\mathbf{M}}$, $\tilde{\mathbf{C}}$, and $\tilde{\mathbf{K}}$ are desired which account for the aforementioned modifications to the transfer function. In [10] the authors walk through the determination of these matrices when looking at non-zero expansion points. In [11] the authors describe how to account for frequency dependency in the system matrices. The details on combining both considerations are presented in [7]. The desired matrices are

$$\begin{aligned} \tilde{\mathbf{M}} &= \mathbf{M} + \boldsymbol{Y}'_s(s_0)\mathbf{D}, \\ \tilde{\mathbf{C}} &= 2s_0\mathbf{M} + s_0\boldsymbol{Y}'_s(s_0)\mathbf{D} + \boldsymbol{Y}_s(s_0)\mathbf{D}, \\ \tilde{\mathbf{K}} &= s_0^2\mathbf{M} + s_0\boldsymbol{Y}_s(s_0)\mathbf{D} + \mathbf{K}. \end{aligned} \tag{12}$$

Here $\mathbf{D}$ is a density-area matrix which results from pulling the admittance function out of the integrals defining a typical acoustic damping matrix [14]

$$\mathbf{C}(s)_{ij} = \boldsymbol{Y}_s(s)\mathbf{D}_{ij} = \boldsymbol{Y}_s(s)\int_{\Gamma_Z}(\rho_0\boldsymbol{N}_i\boldsymbol{N}_j)\,d\Gamma, \tag{13}$$

where $\boldsymbol{N}_i$ and $\boldsymbol{N}_j$ are weighting and shape functions, and ρ_0 is the density of air. Alas, reduced order system matrices and vector representations

$$\begin{aligned} \mathbf{M_r} = \mathbf{V^T M V},\ \mathbf{D_r} = \mathbf{V^T D V},\ \mathbf{K_r} = \mathbf{V^T K V}, \\ \bar{\boldsymbol{b}}_\mathrm{r} = \mathbf{V^T}\bar{\boldsymbol{b}},\ \boldsymbol{p} = \mathbf{V}\boldsymbol{p}, \end{aligned} \tag{14}$$

are arrived at. The vector $\bar{\boldsymbol{b}}$ selects the input DOF, the reduced input vector is represented by $\bar{\boldsymbol{b}}_\mathrm{r}$, the vector of moment coordinates by $\boldsymbol{p} \in \mathbb{C}^{\mathrm{RDOF}\times 1}$, and the reduced system matrices are $\mathbf{M_r}, \mathbf{D_r}, \mathbf{K_r} \in \mathbb{C}^{\mathrm{RDOF}\times\mathrm{RDOF}}$. The aim is to substantially reduce the system DOFs (RDOF $<<$ NDOF) without sacrificing accuracy. The expansion points and moment order were selected using an automated Krylov subspace algorithm, see [21] and [22] for more details.

4 COMBINED APPROACH

Modifications to a standard Newmark-beta integrator [23] ($\gamma = 1/2, \beta = 1/4$) allow the reduced order system to be combined with the TDIBC approach. The steps of the time-stepping scheme are shown in Algorithm 1,

Algorithm 1 Surface Admittance Approach

procedure CALCULATE TIME SERIES( )

Initialize: $\boldsymbol{p}_1 = \dot{\boldsymbol{p}}_1 = \mathbf{0}_{\mathrm{RDOF\,x\,1}}, \quad \boldsymbol{a}_1 = \boldsymbol{\phi}_1^k = \mathbf{0}_{\mathrm{NDOF\,x\,1}}, \quad \ddot{\boldsymbol{p}}_1 = \mathbf{M_r}^{-1}\boldsymbol{f}_1^r,$

with $\quad \boldsymbol{f}_n^r = \bar{\boldsymbol{b}}_\mathrm{r} u_n$

for $n = 1$ to length$(u_n)-1$ **do**

$\boldsymbol{p}'_{n+1} = \boldsymbol{p}_n + \Delta t\dot{\boldsymbol{p}}_n + \frac{\Delta t^2}{4}\ddot{\boldsymbol{p}}_n$ ▷ Initial predictions distinguished by $'$

$\dot{\boldsymbol{p}}'_{n+1} = \dot{\boldsymbol{p}}_n + \frac{\Delta t}{2}\ddot{\boldsymbol{p}}_n$

$\boldsymbol{\phi}_{n+1}^{k'} = \boldsymbol{\phi}_n^k e^{\xi_k \Delta t} - \frac{1}{\xi_k}\left(1 - e^{\xi_k \Delta t}\right)\mathbf{B V}\dot{\boldsymbol{p}}'_{n+1}$

$\boldsymbol{a}_{n+1} = \sum_{k=1}^{N_\xi} \mu_k \boldsymbol{\phi}_{n+1}^{k'}$

$\boldsymbol{r}_{n+1} = \boldsymbol{f}_{n+1}^r - \mathbf{V^T D}\boldsymbol{a}_{n+1} - \mathbf{K_r}\boldsymbol{p}'_{n+1}$ ▷ $\boldsymbol{f}_{n+1}^d = \mathbf{V^T D}\boldsymbol{a}_{n+1}$

$\ddot{\boldsymbol{p}}_{n+1} = \left(\mathbf{M_r} + \frac{\Delta t}{2}\mathbf{C_t} + \frac{\Delta t^2}{4}\mathbf{K_r}\right)^{-1} \cdot \boldsymbol{r}_{n+1}$

$\boldsymbol{p}_{n+1} = \boldsymbol{p}'_{n+1} + \frac{\Delta t^2}{4}\ddot{\boldsymbol{p}}_{n+1}$ ▷ Correct variables

$\dot{\boldsymbol{p}}_{n+1} = \dot{\boldsymbol{p}}'_{n+1} + \frac{\Delta t}{2}\ddot{\boldsymbol{p}}_{n+1}$

$\boldsymbol{\phi}_{n+1}^k = \boldsymbol{\phi}_n^k e^{\xi_k \Delta t} - \frac{1}{\xi_k}\left(1 - e^{\xi_k \Delta t}\right)\mathbf{B V}\dot{\boldsymbol{p}}_{n+1}$

$y_{n+1} = \bar{\boldsymbol{c}}^\mathrm{T}\mathbf{V}\boldsymbol{p}_{n+1}$ ▷ Output

where the variables yet to be introduced are the binary impedance boundary node selection matrix $\mathbf{B}$, the residual $\boldsymbol{r}$, reduced input-force vector $\boldsymbol{f}^r$, the input time series u, output DOF selection vector $\bar{\boldsymbol{c}}$, and the desired output time series y.

5 NUMERICAL VERIFICATION

For numerical verification the test problem mimics the geometry of the KU Leuven Sound Box [24], see Fig. 2 for the interior volume geometry. The input signal is a band-pass filtered impulse (20–550 Hz passband) with the intention to keep the frequency response beneath the maximum frequency dictated by the finite element mesh. The maximum element size was set considering quadratic elements and a conservative six-element per wavelength thumb rule [14] where $f_{max} = 500$ Hz was taken in the calculation. The surface admittance function at the impedance boundary was calculated using the Miki model [25] for a 60 mm layer of mineral wool with a flow resistivity of 32102 Pa·s/m^2 [26]. The surface admittance was fit with four real poles/gains and two complex conjugated pole/gain pairs resulting in relative errors of less than 0.2% across the frequency range under consideration.

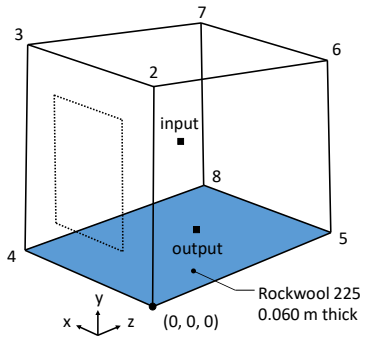

pt.	x [m]	y [m]	z [m]
1	0	0	0
2	0	0.982	0
3	0.778	0.981	0
4	0.815	0	0
5	0	0	1.150
6	0	0.849	1.082
7	0.783	0.848	1.082
8	0.815	0	1.150
in	0.395	0.495	0.561
out	0.290	0.099	0.561

Figure 2: A monopole source is postioned at the input DOF and the response is taken at the output DOF. The table includes the coordinates of the vertices, input DOF, and output DOF. The impedance boundary is set on the bottom of the chamber.

Concerning the model reduction projection basis, expansion point and moment order selection were handled using an automated Krylov subspace algorithm (AKSA) [21, 22]. The resulting reduced-order system based frequency response function (FRF) differs from that of the full-order system by less than 3e-4% over the entire frequency range. The reduced-order system has RDOF $= 63$ degrees of freedom as compared to the full-order system at NDOF $= 13125$ degrees of freedom.

The filtered impulse response for the system, calculated using Algorithm 1, is shown in Fig. 3a. The errors resulting from comparing the full-order and reduced-order system (ROM) responses are plotted in Fig. 3b.

The time series in Fig. 3a are next discrete Fourier transformed (DFT) to compare with the full-order FRF. The FRF was calculated directly in the frequency domain at a 1 Hz resolution. This comparison successfully validates the TDIBC formulation.

Figure 5 affords a closer look at errors relative to the full-order FRF where the various cases represent changes in the time step. The legend includes the sample frequency, f_s, for each case. The time step is set at $1/f_s$. The errors are averaged over 1/3-octave band intervals.

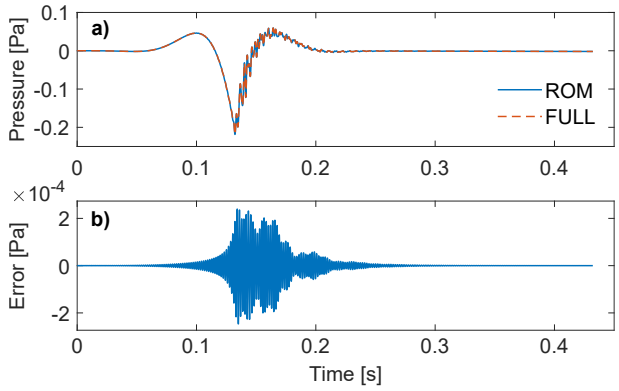

Figure 3: **a)** The filtered impulse response of the chamber for both the full and reduced-order systems. The time step, Δt, is set at $1/f_s$, with $f_s = 44.1$ kHz. **b)** The error between the full-order and reduced-order system responses.

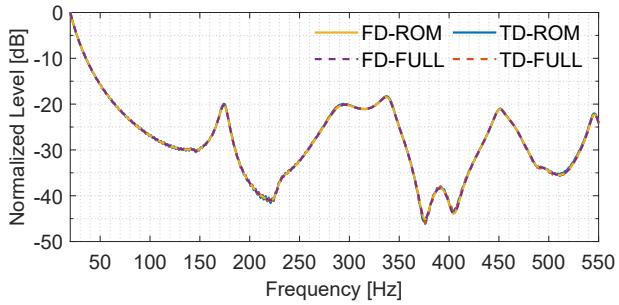

Figure 4: The frequency responses of the chamber for the normalized pressure level. The 'TD' curves were discrete Fourier transformed from time series calculated using Algorithm 1. Direct frequency domain calculation at a 1 Hz resolution yielded the 'FD' curves

5.1 Discussion

The comparison of the results natively calculated in the time domain with the full-order FRF in Fig.'s 4 and 5 demonstrate the accuracy and effectiveness of the TDIBC formulation. Figure 5 demonstrates, as expected, that the accuracy improves with the shortening of the time step. The question of whether or not the errors will result in audible differences is of course perceptual in nature and depends both on the frequency and loudness. Experimental results in [27] indicate a threshold of 0.5 dB over the frequencies considered at present. The desired accuracy and potential for error audibility then dictate the time step size. In [7] the authors show the errors are insignificant as compared to errors introduced by boundary simplifications.

The reduced order model proves to be an accurate representation of the system. The reduced order model has RDOF = 63 DOF while the full-order system has NDOF = 13125 DOF. Both cases require consideration of 457 nodes on Γ_Z. Application of a six-element per wavelength thumb rule [14] with $f_{max} = 500$ Hz determined the number of boundary nodes. The ROM cases resulted in a reduction of simulation time of 91–97% including the offline cost of the basis calculation, see Table 1. The simulations were ran on a personal computer with a 2.60 GHz six-core processor and 16 GB of RAM. Additional simulations were performed using a closely related surface impedance formulation in [7].

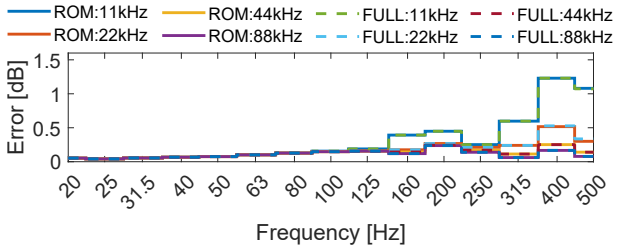

Figure 5: One-third octave band averaged errors calculated relative to the full-order FRF. For the frequency responses originating in the time domain Algorithm 1 was used with time steps set at $1/f_s$, where the nominal sample frequencies are listed.

Table 1: Averaged simulation times where the time steps were set at $1/f_s$. A single reduced-order model is responsible for all ROM cases while a single full-order model was used to calculate the FULL cases.

f_s [kHz]	ROM ($\boldsymbol{Y_s}$) [s]	FULL ($\boldsymbol{Y_s}$) [s]
11.025	32	1488
22.050	61	2854
44.100	115	5470
88.200	240	10566

Calculate ROM: 100 s

6 CONCLUSION

A model order reduction strategy and time-domain impedance boundary condition formulation have been paired to accurately and efficiently simulate an acoustic finite element system. A reduction of simulation times from 91–97% was observed while minimizing the possibility of audible errors. This approach is limited to rigidly backed porous/fibrous impedance boundaries and when the locally-reacting assumption is valid. Future developments may seek to alternatively model the characteristic impedance using an equivalent fluid model as in [28]. Working with a surface impedance function is also possible and is demonstrated in [7]. Working in the time domain requires special handling of convolutions but allows for direct binaural output of the acoustic response.

7 ACKNOWLEDGMENTS

The research of M. Miller III is funded by an Early Stage Researcher grant within the European Project VRACE, Marie Curie Initial Training Network (GA 812719). The research of S. van Ophem is funded by a grant (fellowship no. 1277021N) from the Fund for Scientific Research, Flanders (F.W.O). The Research Fund KU Leuven is gratefully acknowledged for its support.

REFERENCES

[1] C. Zwikker, C. W. Kosten, Simple theory of sound absorption by homogenous layers, in: Sound Absorbing Materials, Elsevier Pub. Co., New York, 1949, pp. 1–3.

[2] A. Semlyen, A. Dabuleanu, Fast and accurate switching transient calculations on transmission lines with ground return using recursive convolutions, IEEE Trans. on Power Appar. and Sys. 94 (2)

(1975) 561–571.

[3] C. K. W. Tam, L. Auriault, Time-domain impedance boundary conditions for computational aeroacoustics, AIAA Journal 34 (5) (1996) 917–923.

[4] Y. Reymen, 3D High-order discontinuous Galerkin methods for time-domain simulation of flow noise propagation, Ph.D. dissertation, KU Leuven, Leuven, BE (2008).

[5] B. Cotté, P. Blanc-Benon, C. Bogey, F. Poisson, Time-domain impedance boundary conditions for simulations of outdoor sound propagation, AIAA J. 47 (10) (2009) 2391–2403.

[6] D. Dragna, P. Pineau, P. Blanc-Benon, A generalized recursive convolution method for time-domain propagation in porous media, J. Acous. Soc. Amer. 138 (2) (2015) 1030–1042.

[7] M. Miller III, S. van Ophem, E. Deckers, W. Desmet, Time-domain impedance boundary conditions for acoustic reduced order finite element simulations, Comput. Methods Appl. Mech. Engrg. (Submitted Feb. 2021).

[8] A. van de Walle, F. Naets, E. Deckers, W. Desmet, Stability-preserving model order reduction for time-domain simulation of vibro-acoustic FE models, Int. J. Numer. Meth. Engrg. 109 (2017) 889–912.

[9] S. van Ophem, O. Atak, E. Deckers, W. Desmet, Stable model order reduction for time-domain exterior vibro-acoustic finite element simulations, Comput. Methods Appl. Mech. Engrg. 325 (2017) 240–264.

[10] B. Salimbahrami, B. Lohmann, Order reduction of large scale second-order systems using Krylov subspace methods, Lin. Alg. and its Apps. 415 (2) (2006) 385–405.

[11] X. Xie, H. Zheng, S. Jonckheere, A. van de Walle, B. Pluymers, W. Desmet, Adaptive model reduction technique for large-scale dynamical systems with frequency-dependent damping, Comp. Methods in Appl. Mech. and Engrg. 332 (2018) 363–381.

[12] Z. Bai, Y. Su, SOAR: A second-order Arnoldi method for the solution of the quadratic eigenvalue problem, SIAM J. Matrix Anal. Appl. 26 (3) (2005) 640–659.

[13] M. Aretz, Combined wave and ray based room acoustic simulations of small rooms, Ph.D. dissertation, RWTH Aachen University, Aachen, DE (2012).

[14] N. Atalla, F. Sgard, Solving uncoupled structural acoustics and vibration problems using the finite-element method, in: Finite Element and Boundary Methods in Structural Acoustics and Vibration, CRC Press, Boca Raton, 2015, pp. 105–191.

[15] B. Gustavsen, A. Semlyen, Rational approximation of frequency domain responses by vector fitting, IEEE Trans. on Power Delivery 14 (3) (1999) 1052–1061.

[16] B. Gustavsen, Improving the pole relocating properties of vector fitting, IEEE Trans. on Power Delivery 21 (3) (2006) 1587–1592.

[17] D. Deschrijver, M. Mrozowski, T. Dhaene, D. De Zutter, Macromodeling of multiport systems using a fast implementation of the vector fitting method, IEEE Microwave and Wireless Comp. Lett. 18 (6) (2008) 383–385.

[18] The *vectfit3.m* MATLAB® routine can found at

https://www.sintef.no/projectweb/vectorfitting/ (Last viewed December 20, 2020).

[19] F. Monteghetti, D. Matignon, E. Piot, L. Pascal, Design of broadband time-domain impedance boundary conditions using the oscillatory-diffusive representation of acoustical models, J. Acoust. Soc. Amer. 140 (3) (2016) 1663–1674.

[20] P. Feldmann, R. W. Freund, Efficient linear circuit analysis by Pade approximation via the Lanczos process, IEEE Trans. Comp.-Aided Des. Integrated Circ. Sys. 14 (5) (1995) 639–649.

[21] A. van de Walle, The power of model order reduction in vibroacoustics and its applications in model-based sensing, Ph.D. dissertation, KU Leuven, Leuven, BE (2018).

[22] S. van Ophem, Novel reduction techniques for exterior vibro-acoustic models and their use in model-based sensing and identification, Ph.D. dissertation, KU Leuven, Leuven, BE (2019).

[23] T. J. R. Hughes, K. S. Pister, R. L. Taylor, Implicit-explicit finite elements in nonlinear transient analysis, Comput. Methods Appl. Mech. Engrg. 17/18 (1979) 159–182.

[24] M. Vivolo, Vibro-acoustic characterization of lightweight panels by using a small cabin, Ph.D. dissertation, KU Leuven, Leuven, BE (2013).

[25] Y. Miki, Acoustical properties of porous materials - Modifications of Delany-Bazley models, J. Acoust. Soc. Jpn. (E) 11 (1) (1990) 19–24.

[26] Typical Rockwool flow resistivities listed in:
https://rti.rockwool.com/siteassets/tools--documentation/documentation/marine-offshore-global/brochures/rti-brochure-searoxacoustic-manual_int_en.pdf
(Last viewed December 2, 2020).

[27] J. Backus, Loudness level: Phons, in: The Acoustical Foundations of Music, W. W. Norton, New York, 1969, p. 86.

[28] F. Pind, C. H. Jeong, A. P. Engsig-Karup, J. S. Hesthaven, J. Strømann-Andersen, Time-domain room acoustic simulations with extended-reacting porous absorbers using the discontinuous Galerkin method, J. Acous. Soc. Amer. 148 (5) (2020) 2851–2863.